Small-angle neutron scattering study of magnetic ordering and inhomogeneity across the martensitic phase transformation in Ni_{50−x}Co_{x}Mn_{40}Sn_{10} alloys

Kanwal Preet Bhatti, S. El-Khatib, Vijay Srivastava, R. D. James, and C. Leighton

Phys. Rev. B **85**, 134450 — Published 27 April 2012

DOI: 10.1103/PhysRevB.85.134450

Revised version re-submitted to *Phys. Rev. B.* on 04/12/12

Small-angle neutron scattering study of magnetic ordering and inhomogeneity across the martensitic phase transformation in $Ni_{50-x}Co_xMn_{40}Sn_{10}$ alloys

Kanwal Preet Bhatti[1], S. El-Khatib[2,3], Vijay Srivastava[4], R.D. James[4] and C. Leighton[1]*

[1] *Department of Chemical Engineering and Materials Science, University of Minnesota, Minneapolis, MN 55455, USA.*

[2] *Department of Physics, American University of Sharjah, PO Box 26666, Sharjah, United Arab Emirates.*

[3] *NIST Center for Neutron Research, National Institute for Standards and Technology, Gaithersburg, MD 20899, USA.*

[4] *Department of Aerospace Engineering and Mechanics, University of Minnesota, Minneapolis, MN 55455, USA.*

The Heusler-derived multiferroic alloy $Ni_{50-x}Co_xMn_{40}Sn_{10}$ has recently been shown to exhibit, at just above room temperature, a highly reversible martensitic phase transformation with an unusually large magnetization change. In this work the nature of the magnetic ordering above and below this transformation has been studied in detail in the critical composition range x = 6-8 via temperature-dependent (5-600 K) magnetometry and Small-Angle Neutron Scattering (SANS). We observe fairly typical paramagnetic to long-range-ordered ferromagnetic phase transitions on cooling to 420-430 K, with the expected critical spin fluctuations, followed by first-order martensitic phase transformations to a non-ferromagnetic state below 360-390 K. The static magnetization reveals complex magnetism in this low temperature non-ferromagnetic

phase including a Langevin-like field dependence, distinct spin freezing near 60 K, and significant exchange bias effects, consistent with superparamagnetic blocking of ferromagnetic clusters of nanoscopic dimensions. We demonstrate that these spin clusters, whose existence has been hypothesized in a variety of martensitic alloys exhibiting competition between ferromagnetic and antiferromagnetic exchange interactions, can be directly observed by SANS. The scattering data are consistent with a liquid-like spatial distribution of interacting magnetic clusters with a mean center-to-center spacing of 12 nm. Considering the behavior of the superparmagnetism, cooling-field and temperature-dependent exchange bias, and magnetic SANS, we discuss in detail the physical form and origin of these spin clusters, their inter-cluster interactions, the nature of the ground state magnetic ordering in the martensitic phase, and the implications for our understanding of such alloy systems.

*Corresponding author: leighton@umn.edu

PACS numbers: 75.50.Cc, 75.25.-j, 75.30.Kz

I. Introduction

Metallic alloys exhibiting a first-order diffusionless phase transformation from a high temperature cubic phase (austenite) to a low temperature phase with lower symmetry (martensite) are abundant, and have attracted attention for decades. Incorporation of *3d* transition metals in such alloys introduces strong exchange interactions, leading to a rich interplay between crystal structure, microstructure, magnetism, and electronic conduction across the martensitic transformation [1]. Both the magnetic moment and the exchange interactions are sensitive to the composition, symmetry, and lattice parameters, meaning that the martensitic phase transformation can trigger a variety of accompanying magnetic transitions such as paramagnetic (P) to ferromagnetic (F), F to antiferromagnetic (AF), or F to F with the two F phases having distinctly different character [1]. Despite this complexity, considerable progress has been made in understanding the phase behavior of such alloys (e.g. Ni-Mn-Sn, Ni-Mn-In) within a framework where the total valence electron density (the e/a ratio) is the primary tuning parameter [2,3].

In addition to thermally-driven first-order magnetic transformations these alloys systems also exhibit multiferroicity (due to the coexistence of ferroelasticity with ferro- or antiferro-magnetism) [1,4], magnetic shape memory effects [1,5], magnetic field-induced phase transformations [1,5], and barocaloric effects [6]. Naturally, this diverse functionality has inspired a variety of potential applications including use of the shape memory effect and field-induced transformations in sensors and actuators [5], and exploitation of the abrupt phase transformation in conventional magnetocaloric [7,8], inverse magnetocaloric [7,8], and energy conversion devices [9].

As well as being of considerable interest from the basic science perspective, the temperature hysteresis at the first-order thermally-driven martensitic phase transformations in these alloys (ΔT_m) also plays a critical role in proposed applications. In many cases (e.g. energy conversion), minimization of ΔT_m is in fact essential in order to achieve efficiency competitive with more traditional approaches (e.g. thermoelectrics) [9]. The physical origin of ΔT_m has thus been the subject of considerable attention, over a sustained period. Despite this prolonged effort, our fundamental understanding of the physical mechanisms controlling hysteresis at martensitic phase transformations is remarkably incomplete. Concepts such as pinning of austenite/martensite interfaces at defects of various types, martensite nucleation and thermal activation, metastability associated with incompatibility, cell volume change, and the importance of a self-organized critical state have all been advanced [as reviewed in refs. 4 and 10], but no single mechanism has been found compatible with the large body of available experimental data.

Recent work has shed much light on this situation by hypothesizing that hysteresis may be controlled, to a significant extent, by novel concepts related to geometrical compatibility between the austenite and martensite unit cells [10]. Specifically, Zhang *et al* [10] conjectured that ΔT_m could be minimized in the situation where an invariant plane exists between the austenite and martensite phases, i.e. an "exact" interface occurs at the austenite/martensite boundary. Mathematically, the condition for such an interface to occur is simply $\lambda_2 = 1$, where λ_1, λ_2, and λ_3 are the ordered eigenvalues of the transformation stretch matrix ($\boldsymbol{U}$) describing the austenite $\rightarrow$ martensite transformation. Most importantly, comprehensive investigations of model (and technologically relevant) alloys such as Ti-Ni-X (where X = Cu, Pd, Pt, or Au) have provided compelling evidence for such a picture, the magnitude of ΔT_m decreasing dramatically

in the composition regions where the lattice parameters dictate $\lambda_2 \approx 1$ [10]. The ΔT_m in fact decreases from 60-70 K to only a few K in the region $\lambda_2 = 1.000 \pm 0.005$. The conjectured "exact" interface between austenite and martensite phases has even been directly observed in high-resolution transmission electron microscopy studies of Ti-Ni-Pd alloys with $\lambda_2 \approx 1$ [11]. There is thus accumulating evidence for the importance of these geometrical compatibility concepts. It should be noted that the theory required to relate λ_2 to ΔT_m has been worked out in some detail, and that arguments for the apparent lack of sensitivity to other factors previously considered important (e.g. volume change) have also been developed [10].

Due to the fundamental interest and considerable application potential of magnetic versions of these alloy systems, the application of these new ideas regarding temperature hysteresis to magnetic alloys has been rapid. For instance, in 2010 Srivastava *et al* [12] reported that, starting from the full Heusler alloy Ni_2MnSn, they were able to tune λ_2 close to 1 via composition control. This was achieved by substituting Co for Ni in the off-stoichiometric Heusler $Ni_{50}Mn_{25+y}Sn_{25-y}$, which had already been shown to exhibit anomalously low ΔT_m [2] and was indeed found to have λ_2 relatively close to 1 at $y \approx 15$. The base $Ni_{50}Mn_{25+y}Sn_{25-y}$ alloy is a good example of a system where the magnetic ground state can be rationally tuned via composition. The ordered full Heusler alloy Ni_2MnSn ($y = 0$) is F with a Curie temperature (T_C) near 350 K [2]. The magnetic moment is understood to be confined mostly to the Mn sites, with strong F exchange interactions between them. Addition of excess Mn then leads to occupation of Sn sites by Mn, which is thought to lead to AF Mn-Mn nearest neighbor exchange interactions [13], providing a means to control the relative strength of F and AF interactions, thus tuning the ground state magnetic ordering [2,14,15], likely via non-collinear spin structures. These AF spin

correlations have been directly observed in $Ni_{50}Mn_{37}Sn_{13}$ by neutron polarization analysis, and are particularly strong in the low T martensitic phase [16]. The substitution of Co on the Ni site by Srivastava *et al* [12] to form the $Ni_{50-x}Co_xMn_{40}Sn_{10}$ alloy was done to tune λ_2 even closer to 1, and to simultaneously increase the magnetization in the austenite phase. The result was the fascinating and potentially useful alloy $Ni_{45}Co_5Mn_{40}Sn_{10}$ having large saturation magnetization (1170 emu/cm^3) and low magnetocrystalline anisotropy in the austenite phase, a non-F martensitic phase with low magnetization, a transformation temperature of approximately 410 K, and remarkably low $\Delta T_m \approx 6$ K. Note the combination of low ΔT_m and very large magnetization change, in a material with a transformation temperature above ambient, which is very desirable for applications. The attractive properties at the analogous composition $Ni_{45}Co_5Mn_{37}In_{13}$ were also identified via an independent experimental effort by Karaca *et al*, who highlighted the exceptional promise of this alloy for sensing, actuation, and refrigeration [5].

The extraordinary magnetic properties of this newly developed $Ni_{50-x}Co_xMn_{25+y}Sn_{25-y}$ alloy were also studied in the work of Cong *et al* in 2010 [17], where a phase diagram was constructed, in the temperature-Co doping plane ($0 \leq x \leq 10$), at a similar Sn content ($y = 11$) to Srivastava *et al* [12]. The martensitic transformation temperature was found to decrease with x, from 400 K at $x = 0$, to below 273 K at $x \approx 8$. As x is increased the magnetism evolved from P austenite and AF [18] martensite (for $x < 5$), to a situation (for $x \geq 5$), where the austenite phase orders F (below a T_C that increases with x), but the martensite exhibits much weaker magnetism, apparently non-F. In the interesting region between 5 and 8 % Co the temperature interval between the T_C of the austenite phase and the martensitic phase transformation widens with x, and the magnetic properties of the martensite phase were found unusually complex. No large

spontaneous magnetization is evident (ruling out a conventional F state), but weak magnetism *is* present, exhibiting features such as distinct low field curvature and clear non-saturation in isothermal hysteresis loops, as well as an obvious (frequency-dependent) freezing point [17,19].

Similar low temperature behavior has been observed in related off-stoichiometric Heusler alloys, such as $Ni_{50}Mn_{25+y}Sn_{25-y}$ [2] and $Ni_{50}Mn_{25+y}In_{25-y}$ [3], near the compositions where the additional Mn, via the mechanism discussed above, leads to destabilization of long-range F order and strong competition between F and AF exchange. The data are typically interpreted in terms of formation of F clusters in a paramagnetic or AF matrix, leading to superparmagnetic phenomena. Although such a picture is capable of explaining the basic behavior there remain many open questions, including the origin of the F clustering (i.e. the magnetic inhomogeneity), the issue of whether the background martensitic matrix is in fact paramagnetic or AF, the spatial range of the F and AF spin correlations, and the true nature of the freezing transition. Regarding the latter issue, it has been suggested, by a number of authors [19,20], that the freezing of the spin clusters is actually collective, obviously requiring strong inter-cluster interactions, leading to a so-called "super-spinglass" state. Additionally, it is now clear, from a number of works [e.g. refs 20-22], that these systems also exhibit exchange bias effects below the blocking point, which can be interpreted as being due to interfacial exchange interactions between short-range F clusters and a long-range AF matrix.

It is hopefully clear from the above that the $Ni_{50-x}Co_xMn_{40}Sn_{10}$ system in the specific composition range x = 5-8 provides a unique opportunity to further our fundamental understanding of magnetism near martensitic phase transformations in the critical phase region

where F and AF exchange interactions are in strong competition. An improved understanding of the multitude of phenomena that emerge in this regime would not only improve our understanding of the basic physics relevant to a wide range of alloy systems, but could also have significant impact on potential applications. To this end, we present here the results of detailed and systematic studies of $Ni_{50-x}Co_xMn_{40}Sn_{10}$ at $x = 6$ and 8. In particular, in addition to standard macroscopic magnetic measurements to characterize the basic magnetic response, we have also performed wide temperature range Small-Angle Neutron Scattering (SANS) measurements with to gather new information on the spatial range of the magnetic correlations, the nature of the magnetic transitions, and the possibility of nanoscale magnetic inhomogeneity. As discussed below, the data provide a wealth of new information on these issues, including the first direct observation of the nanoscopic spin clusters hypothesized to exist in a variety of these alloys.

II. Experimental Details, Sample Preparation, and Structural Characterization

Polycrystalline $Ni_{50-x}Co_xMn_{40}Sn_{10}$ ingots with $x = 6$ and 8 were prepared by arc melting high purity Ni (99.999 %), Co (99.99 %), Mn (99.98 %), and Sn (99.99 %) under a positive Ar pressure. To promote homogeneity the ingot was melted and turned six times, then subsequently annealed in an evacuated quartz vessel at 900 °C for 24 hours and water quenched. Mass loss upon arc melting was verified to be < 1 %. The exact composition was determined via carefully calibrated Energy Dispersive Spectroscopy (EDS). Differential Scanning Calorimetry (DSC) was performed in a commercial Thermal Analyst instrument at heating/cooling rates of 10 K/min between 225 and 475 K. For $Ni_{44}Co_6Mn_{40}Sn_{10}$ such measurements reveal $m_s = 398$ K, $m_f = 388$ K, $a_s = 382$ K, and $a_f = 392$ K, where m_s, m_f, a_s, and a_f are the martensite start, martensite finish, austenite start, and austenite finish temperatures using the standard parameterization of

martensitic phase transformation temperatures. Similar DSC measurements on $Ni_{42}Co_8Mn_{40}Sn_{10}$ reveal m_s = 393 K, m_f = 383 K, a_s = 376 K, and a_f = 386 K. As expected from Cong *et al* [17], the phase transformation temperatures decrease with Co content, x. ΔT_m, was defined as the difference between a_f and m_s, leading to values of 6 and 7 K for $Ni_{44}Co_6Mn_{40}Sn_{10}$ and $Ni_{42}Co_8Mn_{40}Sn_{10}$, respectively. As anticipated for alloys with λ_2 close to 1 (see below), these ΔT_m values are rather low.

Temperature-dependent wide-angle x-ray diffraction (WAXRD) was performed at the Cu K_α wavelength (1.5405 Å) on a Bruker Advance D8 diffractometer. Data were taken from 20 to 100 degrees of scattering angle, with a step size of 0.01 degrees, from room temperature to well above the phase transformation. Representative data sets for $Ni_{44}Co_6Mn_{40}Sn_{10}$ at 410 and 300 K (i.e. above and below the transformation) are shown in Figs. 1(a) and (b) respectively, in addition to the results of a structural refinement using the Bruker TOPAS software. At 410 K we deduce a cubic structure with space group *Fm-3m* and a lattice parameter of 5.987 Å, analogous to the $L2_1$ base Heusler alloy. By 300 K the structure has transformed to a monoclinic *5M*-modulated martensite with space group $P2_1$ having a = 4.407 Å, b = 5.643 Å, c = 21.69 Å and β = 87.05 degrees. Similar results were obtained for $Ni_{42}Co_8Mn_{40}Sn_{10}$, but with slightly different lattice parameters. These lattice parameters result in λ_2 values of 1.0051 and 1.0057 respectively, for $Ni_{44}Co_6Mn_{40}Sn_{10}$ and $Ni_{42}Co_8Mn_{40}Sn_{10}$, consistent with the low ΔT_m.

Specimens cut via electric discharge where used for d.c. magnetometry and SANS. Magnetometry was done in a Quantum Design SQUID magnetometer from 5 to 600 K, in applied magnetic fields from 10 Oe to 70 kOe. For low field measurements the remnant field

profile in the superconducting magnet was measured and the field at the sample nulled to << 1 Oe. SANS data were collected at the NIST Center for Neutron Research on the NG3 instrument at a wavelength of 5.2 Å in a scattering wavevector range of 0.004 $Å^{-1} < q < 0.17$ $Å^{-1}$, using a combination of two sample-detector distances. Data were taken in zero applied field from 30 to 600 K in a high temperature closed-cycle refrigerator.

III. Results and Analysis

The majority of the data presented in this paper are at $x = 6$ (i.e. $Ni_{44}Co_6Mn_{40}Sn_{10}$), and it is this composition we will discuss first. The essential physics is similar at $x = 8$, although the crystallographic and magnetic phase transition temperatures are shifted.

III.1. Magnetometry

The main panels of Figs. 2(a-d) show wide-temperature range (5 K < T < 600 K) magnetometry results at applied magnetic fields (H) of 10 Oe, 5 kOe, 40 kOe and 70 kOe. The left axis plots the d.c. magnetization (M) in emu/cm^3 while the right axis shows the conversion to Bohr magnetons per formula unit (μ_B/f.u.). The data are shown for zero field cooled warming (ZFCW) and field cooled cooling (FCC) conditions. As can be seen from Fig. 2(a), in low H $M(T)$ exhibits a sharp increase on cooling to ≈ 440 K, below which M plateaus. Isothermal $M(H)$ measurements confirm finite remnance (M_R) and coercivity (H_C) in this T range, consistent with the long-range ordered F state thought to occur. The magnetization remains constant down to about 390-400 K (the vicinity of the martensitic phase transformation) at which point it displays a weakly hysteretic transition to a state with low M, indicating that the low T martensitic phase is non-F (e.g. P or AF). As H is increased (Figs. 2(b-d)), $M(T)$ reveals a progressively broadened

onset around T_C, as expected of a second order F $\rightarrow$ P transition. At the same time the martensitic phase transformation temperature decreases with increasing H, reaching 380 K at H = 70 kOe, i.e. at a rate of ≈ -0.3 K/kOe. Although this is qualitatively consistent with the expected field-induced stabilization of the F austenite phase with respect to the non-F martensite, we reserve a quantitative analysis for a subsequent publication [23]. For $H \geq 40$ kOe (Figs. 2(c,d)) the magnetization in the F austenite phase saturates at ≈ 900 emu/cm^3, corresponding to 5 μ_B/f.u. As pointed out in earlier work at x = 5 [12], Co doping results in significantly larger saturation magnetization than the base alloy. This is in agreement with other work [24-27] in that, generally speaking, Co substitution strengthens F interactions. As a point of comparison, the saturation magnetization of $Ni_{50}Mn_{25}Sn_{25}$ is ≈ 600 emu/cm^3 [2]. This point is returned to in section IV.

Although M is low in the non-F martensite phase, close inspection of the low T region in Figs. 2(a-d) clearly indicates that some form of relatively weak magnetism is certainly present. This is shown more clearly in the inset to Fig. 2(a) (a close up of the low T region) which reveals bifurcation of FC and ZFC curves at low H, in addition to a peak in the ZFC $M(T)$ at 60 K. Qualitatively, this behavior, which is consistent with superparamgentic-like freezing at T_f = 60 K, is very similar to that seen in related alloys such as $Ni_{50}Mn_{25+y}Sn_{25-y}$ [2], $Ni_{50}Mn_{25+y}In_{25-y}$ [3,20], and $Ni_{50-x}Co_xMn_{40}Sn_{10}$ [17,19], at compositions where F and AF interactions compete.

Considerable additional information is provided by the isothermal $M(H)$ loops shown in Fig. 3, where each panel captures a specific T regime. Fig. 3(a) illustrates the P $\rightarrow$ F transition on cooling below 440 K, Fig. 3(b) the vicinity of the martensitic phase transformation (390 – 400 K), Fig. 3(c) the non-F martensitic regime, and Fig. 3(d) the region below T_f. Well above T_C (i.e.

the 550 K curve in Fig. 3(a)), a linear response is observed in $M(H)$ as expected for a paramagnet at high T. The 415 K curve shown in Fig. 3(a) is below the T_C indicated by M(T) (Fig. 2(a)) and indeed an F-like hysteresis loop is observed. As shown in the inset finite M_R and H_C are observed, the H_C value of only 15 Oe being consistent with prior work at $x = 5$ concluding that the F austenite possesses quite low magnetocrystalline anisotropy [12]. Fig. 3(b) displays the richer behavior observed in the vicinity of the martensitic phase transformation, i.e. 390 – 400 K. The $M(H)$ loops in this region exhibit the classic behavior associated with field-induced martensitic phase transformation [5]: High H hysteresis due to the field-induced transformation to the F austenitic phase superimposed on a remnant F signature that decreases with decreasing T, as the non-F martensitic phase is entered. More interesting behavior is observed in Fig. 3(c), which focuses on the interval 80 K ≤ T ≤ 370 K, i.e. the non-F martensite phase prior to spin freezing. As T is decreased into this martensitic phase low H non-linearity is observed in $M(H)$ (e.g. at 370 K), superimposed on a linear background. Note that the non-linear F-like contribution is restricted to low fields (H < 5 kOe) for T > 200 K. As T is further decreased, to 150 K and below, more significant non-linearity emerges, extending to much higher H. Finally, as shown in Fig. 3(d), when T is decreased below T_f this non-linearity in $M(H)$ eventually evolves into an open hysteresis loop with significant M_R and H_C. The remnant magnetization turns on at T_f, and increases monotonically with decreasing T.

As discussed above, similar magnetic phenomena in the non-F martensitic phase has been observed in several related alloy systems, and interpreted in terms of some form of superparamagnetic freezing of F clusters. Following the approach of Cong *et al* [17] we thus

fitted $M(H)$ between 60 and 370 K (i.e. the region between T_f and the onset of the martenstic phase transformation) to a Langevin form with an additional linear background:

$$M(H,T) = n_C(T)\mu_C(T)\left[\coth\left(\frac{\mu_C(T)H}{k_BT}\right) - \frac{k_BT}{\mu_C(T)H}\right] + \chi_{BG}(T)H \qquad (1),$$

where n_c and μ_c are the volume density and magnetic moment of the F clusters, and χ_{BG} is the "background" susceptibility of the non-F martensite phase. The resulting fits are shown as solid lines in Fig. 3(c). Equation (1) is found to provide an adequate description of the data in this entire T interval, confirming that the behavior observed can be described by an assembly of thermally fluctuating classical macrospins with negligible anisotropy. The parameters n_c, μ_c, and χ_{BG} extracted from the fitting are shown vs. T in Figure 4. It is observed that, on cooling, μ_c decreases monotonically, n_c increases monotonically, and χ_{BG} exhibits a general increase but with a discontinuity around 100-150 K. In fact, all three quantities are distinctly different above and below about 125 K, as indicated by the vertical dotted line on Fig. 4. We believe that this is due to a simple effect visible in the low field $M(T)$ (Fig. 2(a), inset) and $M(H)$ (Fig. 3(c)). In the low field $M(T)$ for instance it is seen that the decrease in M on cooling into the martensitic phase persists to below 200 K. Similarly, the $M(H)$ data in this T range show a substantial component that saturates at low H. This is likely due to significant volume fractions of *micro*scopic regions of retained austenite. Although the form shown in equation (1) is apparently capable of providing a reasonable description of the total magnetization in this case we do not believe that the extracted parameters are physically meaningful. Below about 100-150 K however the obvious signatures of this *micro*scopic retained austenite are no longer visible in $M(T)$ and $M(H)$, and it can be clearly seen from Fig. 4 that χ_{BG}, μ_c, and n_c enter a new regime. It is in this regime that we believe the extracted parameters are physically meaningful. In particular, μ_c and n_c become T-

independent, taking values of 250 μ_B and 2.6 x 10^{19} cm^{-3}, respectively, similar to the values found by Cong *et al* in $Ni_{43.5}Co_{6.5}Mn_{39}Sn_{11}$ [17].

Rough estimates of the diameter of F particles that would be consistent with these parameters can be obtained by assuming that they are spherical and non-overlapping, with saturation magnetization similar to that observed in the F austenite phase. This process results in an estimated cluster diameter, $d_c \approx 18$ Å. Similarly, the observed cluster density translates into a center-to-center particle spacing ($d_{c\text{-}c}$) of approximately 34 Å, i.e. a mean edge-to-edge separation of ~16 Å. Literal interpretation of these data thus suggests a dense assembly of approximately 20 Å F nanoparticles in a non-F matrix. It must be noted however that these estimates are reliant upon a significant number of simplifying assumptions, such as absence of inter-cluster interactions and cluster overlap, and the assumption of saturation magnetization similar to the bulk magnetization in the austenite. In particular, the saturation magnetization of such a nanoscopic F cluster would be expected to be significantly smaller than the bulk magnetization of 5 μ_B/f.u., due to both finite-size effects and competition between F and AF exchange interactions, which could result in non-collinear spin configurations. This implies that these estimates underestimate d_c. As an example, a cluster magnetization of 1 μ_B/f.u. results in a revised diameter estimate of ≈ 32 Å, while a cluster magnetization of only 0.1 μ_B/f.u. results in ≈ 63 Å. The latter situation (i.e. magnetizations on the order of 0.1 μ_B/f.u.) are what would be expected if the magnetic clusters are not simply F but rather arise from uncompensated AF magnetization. In light of these considerations we view 20 Å as a lower bound estimate for d_c.

An estimate for an upper bound for d_c can be made by utilizing the measured values for T_f and the H_C in the F austenite phase. Based on the Stoner-Wohlfarth model for coherent rotation the H_C that can be obtained for a given uniaxial anisotropy constant, K_u, is bounded by $H_C \leq 2K_u/M_S$, where M_S is the saturation magnetization [28]. In our case the measured H_C value in the F phase is around 15 Oe. Assuming a reasonable H_C^{max} consistent with this value, e.g. 150 Oe, results in an estimated $K_u \sim 1 \times 10^5$ erg/cm^3, quite consistent with the relatively soft character deduced in prior work [12], and with typical values for cubic transition metals [28]. Using the standard Néel-Arrhenius model for the relaxation time, i.e. $\tau = \tau_0 \exp(K_u V/k_B T)$, where $\tau_0 \approx 10^{-9}$ s, and V_c is the cluster volume, we can then estimate an upper bound for V_c (and thus d_c), using the measured T_f of 60 K on the time scale relevant to our $M(T)$ measurement (i.e. 100 s). This results in an upper bound for d_c of ≈ 160 Å, meaning that our simple estimates imply 20 Å < d_c < 160 Å. More direct information on the cluster dimensions, and further discussion of the origin and consequences of the cluster formation is provided below.

In off-stoichiometric Heusler alloys such as $Ni_{50}Mn_{25+y}X_{25-y}$, where X = Sn [22], Sb [21], In [20], etc., it is now well established that exchange bias of the $M(H)$ loops is often observed at low T, at compositions where F and AF exchange interactions compete. This is interpreted in terms of magnetic phase separation into distinct F and AF regions in the martensite phase, a popular scenario being F clusters in an AF matrix [20]. In order to probe the possibility of exchange biasing in $Ni_{44}Co_6Mn_{40}Sn_{10}$, we measured $M(H)$ at 5 K after field-cooling in ± 10 kOe from 300 K (Fig. 5(a)). This corresponds to cooling below T_f, starting from a temperature that is already below the martensitic phase transformation. As can be seen from Fig. 5(a) clear exchange bias is observed, the field shift of the $M(H)$ loop (H_E, about 1 kOe in this case) being in

the opposite sense to the cooling field, as expected. The T dependence of H_E and H_C after application of a strong cooling field (H_{FC} = 70 kOe) are shown in Fig. 5(b). The behavior of $H_E(T)$ is quite typical, the exchange bias decreasing monotonically with increasing T, eventually vanishing at what is typically referred to as the blocking temperature, T_B, about 60 K in this case. The proximity to T_f is obvious, and we thus infer that H_E vanishes at $T_B \approx T_f$ due to loss of static (on the experimental time scale) magnetic order in the nanoscopic clusters. The fact that H_C also exhibits a monotonic decrease with increasing T is interesting, and distinguishes this case from several previous observations in $Ni_{50}Mn_{25+y}X_{25-y}$ (X = Sn, Sb, In) where a strong peak is observed in H_C near T_B [20-22]. Such a peak is common (but not universal) in exchange biased systems and occurs for instance at F/AF interfaces formed between materials with Néel and Curie temperatures such that $T_N << T_C$, and $T_B \approx T_N$ [29]. In this case, as T_N is approached from below the decreasing anisotropy in the AF leads to an increasingly significant restructuring of the AF interfacial spin structure upon reversal of the F, leading to significant energy loss in the AF and thus enhanced H_C [29]. When the AF order is lost at T_N this effect decreases, leading to a peak in H_C around T_N. As can be seen from Fig. 5(b) this effect is clearly *not* present in our case.

There are two important points to make in connection with the absence of a peak in $H_C(T)$. The first is that the data of Figs. 5(a,b) are entirely consistent with a scenario where nanoscopic F clusters exist in a long-range ordered AF matrix. In this situation, which would be realized for instance if the martensitic phase was dominated by AF order, the vanishing of H_E at T_B would be solely due to thermal instability of the nanoscopic F clusters and would be essentially unrelated to the AF order parameter. Under such a circumstance no peak in $H_C(T)$ at T_B would be expected. This is somewhat analogous to AF/F bilayers with $T_C < T_N$, a situation

that has been investigated in detail [30] and shown to result in monotonic $H_C(T)$. Second, and perhaps more generally, detailed work on AF/F bilayered systems [31] has shown that the existence of a peak in $H_C(T)$ at T_N in systems with $T_N << T_C$ depends on the relative thermal stabilities of the F and AF components. In particular, in the case where the thermal stability of the F component is low relative to the AF (i.e. low F volume and/or magnetocrystalline anisotropy), the magnetization reversal in the F is facile and does not induce significant rearrangement of the AF spin structure, and thus no peak occurs in H_C at T_N [31]. Both of these points indicate that the behavior seen in Fig. 5(b) is consistent with a picture where nanoscopic F clusters, on the verge of thermal stability, are embedded in a long-range ordered AF matrix.

The H_{FC} dependence of H_E and H_C was also measured and is shown in Fig. 5(c) at $T = 5$ K. (Note that at $H_{FC} = 0$, no special effort was made to demagnetize the sample; we did not attempt to study the H_E after cooling from an unmagnetized state as in ref. [20]). As is common in F/AF systems with F interfacial exchange interactions [32], $H_E(H_{FC})$ is non-monotonic. The initial increase in H_E occurs due to improved polarization of the cluster magnetizations, the field scale for this process (≈ 5 kOe) being consistent with the saturation of the low T magnetization in $M(T)$ (Figs. 2(c,d)) and the saturation of the F component visible in the low T hysteresis loops (Fig. 3(d)). The $H_C(H_{FC})$ data exhibit a significant decrease in this region, as expected. Above about 10-20 kOe H_C becomes relatively independent of H_{FC}, while H_E exhibits a factor of 2 decrease. This can be interpreted in terms of two effects; a potential increase in cluster size at large H_{FC} (analogous to increasing F thickness in F/AF bilayers, decreasing the importance of interface-induced anisotropies), and high field modification of the AF spin structure. These have been discussed in detail for $Ni_{50}Mn_{25+y}In_{25-y}$ [20].

To summarize the conclusions from the x-ray and magnetometry measurements of Figs. 1-5, it is clear that the high T austenite phase of $Ni_{44}Co_6Mn_{40}Sn_{10}$ is F, that it exhibits a weakly-hysteretic first-order martensitic phase transformation to a low T monoclinic phase, and that this low T phase, clearly not a long-range ordered F, exhibits some form of superparamagnetism. The superparamagnetic behavior is consistent with the existence of nanoscopic magnetic clusters in a non-F matrix, and it is clear, both from the global magnetic phase behavior and the existence of exchange bias, that AF and F exchange interactions are in strong competition. However, the true nature of the magnetic order in the martensite phase, the size, form and origin of the nanoscopic clusters, and the exact source of the exchange biasing remain unclear. In order to probe these issues directly we performed a detailed T-dependent study using SANS.

III.2. Small-Angle Neutron Scattering

The total absolute SANS cross section, $d\Sigma/d\Omega$, is shown in Fig. 6 as a function of scattering wavevector, q, at five specific temperatures, representative of the various important regimes. The data, which were taken in zero applied field, are shown as the points (with error bars), while the lines represent the subsequent analysis of the various contributions to the total scattering intensity (see below). Note that the scattering was isotropic in the q_x-q_y plane and was radially averaged to obtain $d\Sigma/d\Omega$ vs. q. Starting at 500 K, i.e. the P austenite phase well in excess of T_C, we observe behavior that is fairly typical of a coarse-grained polycrystalline paramagnet. There are essentially two contributions to the scattering. At low q (below about 0.02 $Å^{-1}$) the data are well described by a straight line on these log-log plots, indicating power law scattering. This is Porod scattering [33], given by:

$$\frac{d\Sigma}{d\Omega}(q,T) = \frac{\left(\frac{d\Sigma}{d\Omega}\right)_P(T)}{q^n} \qquad (2),$$

where $(d\Sigma/d\Omega)_P$ is a constant parameterizing the strength of the Porod contribution, and n is an exponent that provides information on the nature of the scattering centers. Equation (2) is valid in the limit $q >> 2\pi/D$, where D is the size of the scattering object. The case $n = 4$ (i.e. $d\Omega/d\Sigma \propto q^{-4}$, the Porod Law) is commonly observed [33], describing the scattering from an assembly of 3D objects with "smooth" surfaces. Three dimensional objects with "rough" or "wrinkled" surfaces on the other hand are known to result in $n < 4$, the special value of $n = 3$ marking the transition between surface and volume fractals [34]. In our case the line shown in the low q region of Fig. 6(a) has $n = 4.01$, indicating good adherence to the Porod Law expected for 3D scattering centers with smooth surfaces. As in prior work on a wide variety of materials we interpret this as scattering from grains and grain boundaries. The adherence to this form down to $q = 0.005$ Å^{-1} indicates that these grains are >> 100 nm in size, consistent with microscopy.

In the high q region of Fig. 6(a), i.e. above about 0.02 Å^{-1}, the Porod scattering gives way to distinctly different behavior. The dashed line in Fig. 6(a) is in fact a fit to the well-known Lorentzian form [35],

$$\frac{d\Sigma}{d\Omega}(q,T) = \frac{\left(\frac{d\Sigma}{d\Omega}\right)_L(T)}{q^2 + \left(\frac{1}{\xi(T)}\right)^2} \qquad (3),$$

where $(d\Sigma/d\Omega)_L$ is a constant parameterizing the strength of the Lorentzian scattering, and ξ is the magnetic correlation length. This is the form widely used to describe the scattering from the spin correlations that grow in spatial extent and temporal coherence as a second order magnetic

phase transition temperature is approached from above. Specifically, this results from an Ornstein-Zernike real space spin-spin correlation function, i.e. $\langle S(0), S(r) \rangle \propto e^{-r/\xi} / r$, where ξ is the range of the correlations [36]. Scattering of the form shown in equation (3) is thus expected at 500 K in this material, and provides a direct measure of the spin correlation length.

As T is decreased down to 425 K (Fig. 6(b)), i.e. just above T_C, the Porod scattering from the grains changes little, as expected. The high q Lorentzian scattering increases significantly however, due to the approach to T_C. On cooling to 390 K (Fig. 6(c)) the F phase is entered and the nature of the scattering changes dramatically. The low q regime remains approximately Porod-like but with distinctly larger intensity ($(d\Sigma/d\Omega)_P$) and lower exponent (n). Indeed, in the F phase we find $n \approx 2$, indicating that the scattering arises from objects with rougher surfaces than the structural grains. As in prior work on a wide variety of ferromagnets we interpret this as scattering from F domains, $n < 4$ indicating that the domain walls are not smooth due to pinning at defects [34]. Observation of Porod scattering down to 0.005 $Å^{-1}$ implies that these domains are >> 100 nm in size, clearly illustrating the long-range nature of the F state. The second major change in the F regime (aside from the expected decrease in high q scatter as T falls below T_C), is the emergence of an unexpected hump in the vicinity of 0.04 $Å^{-1}$. When T is further reduced to 380 K (Fig. 6(d)), i.e. the verge of the transition to the martensitic phase, the low q Porod scattering remains largely unaltered (as expected), the high q Lorentzian contribution decreases further (also expected), and the hump around 0.04 $Å^{-1}$ in Fig. 6(c) becomes more obvious. Finally, at 30 K, deep in the non-F martensite phase, further changes occur. The nature of the Porod scattering is again altered, $(d\Sigma/d\Omega)_P$ decreasing cf. the F phase and the exponent abruptly changing to $n \approx 3$, observations that will be discussed later in connection with the magnetic

ground state in the martensite. The final change regards the hump observed around q = 0.04 Å^{-1} in Figs. 6(c,d) which is found to become a clear peak at 30 K, shifting to slightly higher q.

The central question at this stage is the origin of the peak in $d\Sigma/d\Omega(q)$. The fact that the peak emerges only at low T and has a significantly T-dependent magnitude and position is strongly suggestive that it is magnetic in origin. Moreover, Figs. 6(b-e) show that the q values at which this peak occurs lie in the range 0.03 to 0.05 Å^{-1}, corresponding to real space length scales ($2\pi/q$) of 120 to 200 Å. Given the concrete evidence for formation of nanoscopic magnetic clusters in this material at low T (from magnetometry), and the obvious similarity between the length scales deduced from magnetometry and those corresponding to the scattering peak, we conclude that this peak is indeed due to the spin clusters. A close examination of the T dependence of the scattering (see below) provides further support for this interpretation.

Established theory for the SANS expected from assemblies of approximately spherical and monodisperse scattering objects provides additional insight into exactly what information can be extracted from the peak in $d\Sigma/d\Omega(q)$. Generally,

$$\frac{d\Sigma}{d\Omega}(q) = N_P V_P^2 \Delta\rho^2 F(q) S(q) \qquad (4),$$

where N_P and V_P are the number density and volume of the particles, $\Delta\rho$ is the scattering contrast between the particles and the matrix (magnetic in this case), $F(q)$ is the particle form factor and $S(q)$ is the (inter-particle) structure factor [33]. The q dependence of the scattering can thus arise from either $F(q)$, $S(q)$, or both. In the case where the particles are dilute, or randomly oriented, peaks in $d\Sigma/d\Omega(q)$ arise from $F(q)$, which, for spherical particles, is given by,

$$F(q) = \left[\frac{3[Sin(qR) - qRCos(qR)]}{(qR)^3} \right]^2 \qquad (5),$$

where R is the particle diameter [33]. This results in a series of maxima in $d\Sigma/d\Omega(q)$ at $q \approx (p + ½)\pi/R$, where p is an integer [33]. Attempts to explain the *single* peak we observe in Figs. 6(b-e) in terms of this $F(q)$, even allowing for the possibility that additional peaks are either obscured by other scattering contributions, or fall outside the measured q range, are not successful. Alternatively, in the case where the position of the particles is correlated, F takes on a q dependence, resulting in diffraction peaks. Even in the case of only approximate short-range organization this leads to a diffraction-like peak at $q \approx 2\pi/d_{c\text{-}c}$. This is in fact common in systems where F particles exist in some matrix with distinct magnetic order, such as magnetic nanoprecipitates in non-magnetic metal matrices [37], surfactant-coated assemblies of metallic nanoparticles [38,39], or magnetically phase-separated complex oxides [40]. From the peak position at low T (Fig. 6(e)) we thus determine $d_{c\text{-}c} \approx 2\pi/(0.05\ \text{Å}^{-1}) \approx 120$ Å, certainly consistent with our magnetometry estimates for d_c. Fitting to models based on a liquid-like spatial distribution of spherical particles can in principle yield additional information such as cluster size, density, and magnetic contrast with the matrix [40-42]. However, in our case the existence of a single peak with relatively low intensity cf. other contributions indicates that the peak is essentially dominated by $F(q)$ (i.e. $d_{c\text{-}c}$) and is thus unlikely to yield meaningful information on d_c. More information can be extracted from the peak width however, as discussed below.

Before proceeding to a detailed discussion of the T dependence of the parameters in equations (2)-(4), it is worthwhile to simply examine the T dependence of the intensity at certain q values. In particular, $q = 0.005\ \text{Å}^{-1}$ (corresponding to a length scale of ≈ 1200 Å) and $q = 0.1$ Å^{-}

[1] (corresponding to ≈ 60 Å) are illustrative as they lie (see Figs 6(a-e)) in the low q Porod and high q Lorentzian/Gaussian regimes, respectively. The T dependence of the total scattering cross section at these special q values is shown in Fig. 7. Two data sets are shown, one taken on warming from 30 to 500 K, and a second on cooling from 500 to 350 K. Note that this is the total SANS cross section; no attempt has been made to isolate the magnetic contribution by subtracting a structural "background". Starting with the q = 0.005 Å^{-1} case (Fig. 7(a)) we see that the intensity is essentially constant on cooling from 500 K down to 425 K (T_C), at which point it exhibits a rapid increase due to the onset of Porod scattering from long-range F domains. This domain scattering increases down to 380-390 K, at which point the martensitic phase transformation occurs, and the intensity abruptly drops. Although the scattering intensity in the non-F martensitic phase (29.5 to 31.0 cm^{-1}) is much lower than in the F austenite phase it is important to note that is, nevertheless, distinctly larger than in the P region above T_C, where the average intensity is only 25.0 cm^{-1}. It is therefore clear that the low T martensite presents additional scattering in comparison to the P austenite. Quantitative analysis of the T dependence of the Porod fit parameters (see below) provides more insight.

At q = 0.1 Å^{-1} (Fig. 7(b)) the scattering cross section increases immediately on cooling from 500 K, reaching 0.3 cm^{-1} at 425 K, i.e. T_C. Below this the intensity falls quickly, reaching very low levels at the martensitic phase transformation temperature of 380-390 K. The peak thus formed around T_C is the so-called critical scattering peak, an expected feature at a second order F → P transition [36]. Essentially, the increase in scattering as $T \rightarrow T_C^+$ results from the onset of spin correlations as the ordering temperature is approached, while the increase as $T \rightarrow T_C^-$ is due to spin excitations. The result is a strong peak at T_C, which is quite asymmetric for

$Ni_{44}Co_6Mn_{40}Sn_{10}$. At this q value the scattering in the low T martensitic phase is weak but non-zero. In fact, as can be seen upon close inspection of Fig. 7(b), and more clearly in the close-up of the low T region shown in the inset, this weak scattering exhibits a remarkable T dependence. The scattering cross-section is relatively constant down to 130 K, at which point it undergoes an increase reminiscent of a magnetic order parameter. This behavior is not specific to the exact choice of q. Rather, it is seen for any q value in the approximate range 0.02 to 0.1 Å, i.e. any q value in the vicinity of the peak emerging in $d\Sigma/d\Omega(q)$ at low T (Fig. 6). Given that we ascribe this peak to scattering from the nanoscopic spin clusters, the apparent ordering shown in the inset to Fig. 7(b) must therefore be associated with these clusters, an important conclusion.

In order to probe these issues quantitatively we fitted $d\Sigma/d\Omega(q)$ at each T value using:

$$\left(\frac{d\Sigma}{d\Omega}\right)_{Tot}(q,T) = \frac{\left(\frac{d\Sigma}{d\Omega}\right)_P(T)}{q^n} + \left(\frac{d\Sigma}{d\Omega}\right)_G(T)\exp\left(\frac{-(q-q_G(T))^2}{2\Delta(T)^2}\right) + \frac{\left(\frac{d\Sigma}{d\Omega}\right)_L(T)}{q^2+\left(\frac{1}{\xi(T)}\right)^2} \quad (6),$$

i.e. a simple sum of Porod and Lorentzian contributions defined in equations (2) and (3) with an additional Gaussian to capture the peak due to the nanoscopic clusters. Here $(d\Sigma/d\Omega)_G$ is the magnitude of the Gaussian peak, q_G is the peak position, and Δ is the peak width. Although the number of fitting parameters is significant it is essential to note that in the T regions where these contributions are important they are individually dominant in the low q, intermediate q, and high q regions, respectively, meaning that the extraction of the parameters is robust. This was borne out by careful fitting of the individual contributions in the relevant q regimes using equations (2), (3) and a Gaussian separately, a process that yields essentially identical parameters. The final fits

are shown by the solid dense lines in Fig. 6, where it can be seen that the data are described well by equation (6) at all T. The extracted fitting parameters are shown vs. T in Fig. 8.

Figs. 8(a) and (b) show the Porod constant ($(d\Omega/d\Sigma)_P$) and exponent (n). As mentioned above we find $n = 4$ above T_C, i.e. the Porod Law, which we interpret in terms of scattering from grains with smooth boundaries in the P austenite phase. On cooling below T_C we find an immediate increase in $(d\Omega/d\Sigma)_P$, coincident with a sharp decrease in n to a minimum value around 2 at 415 K. This is due to strong scattering from long-range ordered F domains, the observation of $n < 4$ indicating that the domain wall regions are irregularly shaped due to pinning by defects [34]. Upon further cooling into the low T martensitic phase, the nature of the Porod scattering changes abruptly once more. $(d\Omega/d\Sigma)_P$ decreases significantly, while n increases to ≈ 3. It is clear from these data that the Porod scattering in the non-F martensite and the P austenite are significantly different. Additionally, close inspection of the low T martensite region in Fig. 8(a) reveals that although the T dependence is weak, the Porod scattering in this region *is* T dependent. Both this T dependence (a weak decrease with increasing T), and the dissimilarity to the P regime, argue that the scattering in the martensitic phase is not just structural but has at least some magnetic component. To be explicit, scattering due to the twin structure in the martensite likely contributes, but we believe that the total intensity also includes a magnetic contribution. Given that adherence to the Porod form persists to < 0.005 $Å^{-1}$ (e.g. Fig. 6(e)), this magnetism is long-range (>> 1200 Å). When placed in the context of the other observations in this paper, we believe this points to long-range AF order in the martensite.

Figs. 8(c) and (d) show the T dependence of the Lorentzian scattering intensity ($(d\Omega/d\Sigma)_L$) and magnetic correlation length, ξ. As expected this contribution is large only in the P region above T_C, although it must be pointed out that a weak Lorentzian contribution persists to the lowest T. The extracted spin-spin correlation length is finite and already T-dependent at the highest measured T (i.e. 500 K), and increases quickly as $T \rightarrow T_C^+$. The solid line in Fig. 8(d) is a fit to $\xi = \xi_0(T/T_C - 1)^{-\nu}$, where ξ_0 is a constant and ν is a constant exponent, i.e. the standard description of the divergence of the correlation length at a second order magnetic phase transition [35,36]. The fit shown in Fig. 8(d) results in $\nu = 0.42$. This differs from the expected value for 3D Heisenberg and Ising ferromagnets ($\nu = 0.71$ and 0.63, respectively), although it must be noted that the data set in the vicinity of T_C is relatively sparse in comparison to those obtained in detailed phase transition studies.

Figs. 8(e) and (f) show the T dependence of the parameters associated with the peak due to the spin clusters, which is well described by a Gaussian. Fig. 8(e) displays $(d\Omega/d\Sigma)_G$, while Fig. 8(f) presents q_G (left axis) and Δ (right axis). $(d\Omega/d\Sigma)_G$ exhibits a particularly interesting T dependence. This scattering contribution first emerges on cooling through T_C, grows with decreasing T, then undergoes a large hysteretic decrease on cooling into the non-F martensite phase. At the lowest T $(d\Omega/d\Sigma)_G$ is only about 10 % of its maximum value, but it is clearly non-zero. Moreover, it is T-dependent. This point is reinforced by the inset to Fig. 8(e) which shows a blow-up of the low T region. The behavior is very similar to that seen in the inset to Fig. 7(b), confirming our earlier assertion that the magnetic transition seen by neutrons at 130 K is indeed associated with the scattering peak, which we believe is due to nanoscopic spin clusters. Following our interpretation of this peak as a diffraction-like contribution associated with the

mean center-to-center separation of a liquid-like distribution of clusters, the peak width, Δ, provides information on the spatial range of these correlations, although variations in intercluster spacing may also contribute. As shown in Fig. 8(f) both Δ and q_G are T-dependent. On cooling into the low T martensitic phase q_G increases weakly, while Δ decreases by a factor of 5 from 0.05 $Å^{-1}$ to 0.01 $Å^{-1}$. (Note that the experimental q resolution lies well below these values). This Δ corresponds to magnetic correlations over a length scale ($\approx 2\pi/\Delta$) exceeding 600 Å below 350 K. This amounts to ~5 center-to-center spacings, the obvious implication being that the clusters are magnetically interacting. This is important in the context of prior work claiming collective freezing into a super-spinglass state.

It must be emphasized that $\Delta(T)$ exhibits no obvious change in the vicinity of 130 K, demonstrating that the magnetic transition related to the spin clusters at this T is *not* related to the range of the inter-cluster interactions. One possibility is that this transition is nothing other than a form of superparamagnetic blocking. SANS provides access to an unusual regime in this context [43] as the time scale associated with the measurement, whether one considers the residence time of the neutron in a single particle, or the expected energy window over which the measurement integrates, is of order 10^{-11} – 10^{-12} s. It is thus faster than typical attempt frequencies in the standard description of Néel-Arrhenius relaxation (10^9-10^{10} Hz). While we are not aware of any theory developed for this situation we believe that it is plausible that the 130 K transition we observe via neutron scattering in the insets to Figs. 7(b) and 8(e) is nothing other than the T_f detected at 65 K in the quasi-static measurements of Fig. 2. In the regime above 10^9 – 10^{10} Hz we do not believe that extrapolation from lower frequency measurements such as a.c. susceptibility will be valid, and it is thus unclear how one could quantitatively test our hypothesis

that the transition observed in SANS is associated with single particle blocking. More discussion of these points is provided in section IV.

III.3. $Ni_{42}Co_8Mn_{40}Sn_{10}$

As discussed in the introduction, in this work we have specifically targeted the $Ni_{50-x}Co_xMn_{40}Sn_{10}$ system in the range x = 5-8. The data discussed above was collected at x = 6. In Fig. 9 we provide a summary of the similar behavior obtained at x = 8, i.e. $Ni_{42}Co_8Mn_{40}Sn_{10}$, in order to demonstrate the generality of our results and conclusions. Fig. 9(a) shows $M(T)$ at H = 5 kOe, Figs. 9(b) and (c) display the T dependence of the SANS cross section at low and high q (0.01 and 0.1 Å^{-1}, respectively), and Fig. 9(d) presents $\xi(T)$ extracted from the Lorentzian contribution above T_C. Aside from the decreased martensitic phase transformation temperature (Figs. 9(a-c) indicate that this now occurs in the 365-380 K range, cf. 390-400 K at x = 6 (Fig. 2)), the general behavior is similar. In particular, note the sharp onset in low q scattering (Fig. 9(b)), the critical scattering peak (Fig. 9(c)), and the rapidly increasing magnetic correlation length as $T \rightarrow T_C^+$. Indeed, $d\Sigma/d\Omega(q)$ (data not shown) is very similar to x = 6 in the various T regimes, again being composed of Porod, Gaussian, and Lorentzian contributions in the low, medium, and high q ranges, respectively. With regard to the interesting behavior in the low T martensitic phase note that $M(T)$ again exhibits a low T tail with FC/ZFC splitting (Fig. 9(a)), a peak in the ZFC $M(T)$ (Fig. 9(a)), and a weak but significant low T increase in the high q scattering (Fig. 9(c)). These observations are all consistent with some form of superparamagnetic freezing associated with nanoscopic magnetic clusters, again observed directly by SANS. We find T_f = 70 K at this composition (from magnetometry), slightly increased cf. x = 6. The Gaussian SANS peak at the lowest measured temperature (30 K) occurs at q_G = 0.045 Å^{-1} with a

width of 0.014 Å^{-1}. These values correspond to $d_{c\text{-}c}$ = 140 Å and magnetic correlations over ~3.5 center-to-center spacings. This suggests slightly larger clusters than at x = 6 (consistent with the increased T_f, i.e. improved thermal stability) and weaker inter-cluster interactions.

IV. Discussion

While immediate conclusions from individual measurements have already been presented, there are a number of additional conclusions and points of discussion that emerge from examining the data as a whole. First amongst these is the true nature of the magnetic ordering in the low T martensitic phase. Based on the data presented here, and the phase behavior seen in studies on related alloys [2,3], long-range AF or simple paramagnetism are the most likely possibilities. Given our observation in the martensitic phase of significant T-dependent low q Porod scattering with dissimilar characteristics to that seen in the high T paramagnetic phase (Figs 8(a,b)) we believe that the most likely possibility is a long-range ordered AF ground state at x = 6. This hypothesis is also consistent with the existence of exchange bias at low T, which would be expected if F clusters form in an AF martensite matrix. The specific form of $H_E(T)$ and $H_C(T)$ (Fig. 5(b)) are also consistent with this interpretation in that H_E seems to vanish when static F order is lost in the clusters (with no peak in $H_C(T)$), the long-range AF order persisting above this point (up to the martensitic phase transformation we expect). Nevertheless, it must be emphasized that these inferences are indirect. It is clear that neutron powder diffraction is urgently required to unambiguously determine the martensite spin structure.

In any case it is clear that tour results, as well as those of others, unambiguously indicate formation of nanoscopic magnetic clusters in a non-F matrix. At first sight this occurs in a

martensitic state with a single chemical and crystallographic phase, directly implying magnetic phase separation, i.e. spatial coexistence of distinct magnetic phases in a single chemical phase. It is interesting to note that these alloy systems share some intriguing similarities with better-known examples of materials exhibiting magnetic phase separation, such as the intensively studied manganites and cobaltites [44,45]. In particular, the magnetic phase separation occurs in regions of the phase space where F and AF ground states are brought into acute competition via compositional tuning, similar to manganites [44,45]. Significant additional work will be required to determine whether the phase separation in these alloys is purely electronic, or whether the distinct magnetic/electronic phases also exhibit subtle structural or chemical distinctions [46].

Having obtained direct experimental evidence for the existence of these nanoscopic spin clusters, it is obviously important to consider the fundamental origin of these magnetic inhomogeneities. In this context, we believe the T dependence of the cluster scattering shown in Figs. 8(e) and (f) is very important. In particular, the data of Fig. 8(e) reveal that the Gaussian intensity related to these clusters is found to emerge not at the martensitic phase transformation temperature, but rather in the vicinity of the T_C of the austenite phase. In fact, this intensity is found to emerge gradually, over a significant T range, perhaps extending even beyond T_C (Fig. 8(e)). The strength of this scattering contribution increases on cooling to the martensitic phase transformation at which point it drops quickly. In the martensitic phase the peak intensity is constant down to 130 K at which point it undergoes the transition we have ascribed to single particle blocking. One scenario that is consistent with the surprising T dependence of $(d\Sigma/d\Omega)_G$ is that local nano-regions with anomalously strong F behavior emerge at high T (i.e. the bulk T_C or even slightly above). Such regions would present magnetic SANS due to their magnetization-

based contrast with the F matrix with average magnetization, i.e. non-zero magnetic $\Delta\rho$ in equation (4). If the F in these nanoregions were stabilized to a sufficient extent they could persist below the martensitic phase transformation as the long-range F behavior transitions to AF order in the bulk of the sample. These nanoscale F regions would then exhibit superparamagnetic freezing at lower T, as observed. Indeed, we believe this scenario is qualitatively consistent with all observations made here. Given our observation of correlation lengths of order 5 inter-cluster separations it is clear that these clusters are dense enough to strongly interact, giving credence to prior claims of collective effects. Indeed, in the context of the work of Wang *et al* [20] it would be very interesting to perform further H-dependent SANS experiments to test the model for the exchange bias after cooling from an unmagnetized state. Obviously, one critical issue is the driving force for nucleation of nanoclusters with anomalously stable F. Given the nature of these alloys, spatial fluctuations in composition are an obvious culprit, local Co-rich or Mn-poor regions being obvious candidates. Given our specific alloy composition ($Ni_{50-x}Co_xMn_{40}Sn_{10}$), Co-rich nanoclusters are particularly relevant possibilities as it is known that Co substitution leads to rapid stabilization of F exchange interactions [12,17,19,24-27]. Future neutron scattering studies made as a function of Co content, perhaps combined with detailed nanoscale chemical characterization, would be very useful in assessing the validity of this picture.

This brings us to the overall trends in magnetic phase behavior with composition in $Ni_{50-x}Co_xMn_{40}Sn_{10}$. The first thing to point out in this regard is that the decrease in martensitic phase transformation temperature and increase in T_C with x are in qualitative agreement with the phase diagram of Cong *et al* [17]. Some quantitative details may differ, but this could be due to the very slight differences in Sn content between the work of Cong *et al* (Sn_{11}) and our own (Sn_{10}).

An additional piece of information derived from the current work is that T_f apparently increases with x, growing from 60 K at x = 6 to 70 K at x = 8. A detailed phase diagram will need to be established in order to understand the behavior at higher x, but it appears possible that the $T_f(x)$ line marking the onset of superparamagnetic cluster freezing could intersect with the martensitic phase transformation. This is in fact but one of the many interesting issues that could be settled by establishing a detailed phase diagram of this compound. Others include understanding the details of the crossover from an AF to F ground state, and, vitally, possible correlations between the occurrence of F austenite and the existence of superparamagnetic behavior at low T due to formation of nanoscopic spin clusters. It must be noted however that, qualitatively speaking, the major features of the evolution of the phase behavior with Co substitution can be understood in terms of the $Ni_{50}Mn_{25+y}Sn_{25-y}$ phase diagram. Specifically, in the $Ni_{50}Mn_{25+y}Sn_{25-y}$ case, increasing y leads to an increase in the e/a ratio, a crossover from an F to an AF ground state, and an increase in martensitic phase transformation temperature [2]. In the $Ni_{50-x}Co_xMn_{40}Sn_{10}$ case Co substitution *decreases* e/a, leading, as one would then expected, to stabilization of F and a decrease in the martensitic phase transformation temperature. Although more detailed work will be required to assess the extent to which e/a can be viewed as a common tuning parameter, this does provide some basis for rationalizing the increase in the stability of F with Co doping.

As a final comment on the overall magnetic behavior we note that there are reasons to suspect that the P $\rightarrow$ F phase transitions occurring on cooling in $Ni_{50-x}Co_xMn_{40}Sn_{10}$ may not lie deep in a regime where they are of conventional second order type. In particular, Figs. 2(a), 7(a), 8(a) and 9(b) all provide some evidence that the F $\rightarrow$ P transition is anomalously sharp. As touched upon earlier in this paper the critical scattering peaks are also quite asymmetric (see

Figs. 7(b) and 9(c)), and the divergence of the magnetic correlation length is atypical. Additional work will be required to determine whether there are regions of the phase space where this system moves towards a tricritical point, or even first order F $\rightarrow$ P transitions, which would open up the intriguing possibility of multiple martensitic phase transformations.

V. Summary

We have presented detailed magnetometry and small-angle neutron scattering data on polycrystalline $Ni_{50-x}Co_xMn_{40}Sn_{10}$ alloys at x = 6 and 8. This is a critical composition range where ferromagnetic and antiferromagnetic exchange interactions exist in close competition, the magnetic properties of the martensite indicate some form of superparamagnetic freezing of nanoscopic spin clusters of unknown origin, and the overall magnetic properties are closely matched to the needs of multiple applications. In addition to providing detailed characterization of the various temperature-dependent magnetic phase transformations, the small-angle scattering data provide the first direct observation of the nanoscopic magnetic clusters thought to exist at low temperatures in this, and several other related alloy systems. Taken together with a detailed analysis of the magnetometry results (including the observed exchange biasing) the data reveal a wealth of new information on this nanoscale magnetic inhomogeneity including the spatial distribution of clusters, their mean spacing and diameter, the nature of the magnetic order in the martensite matrix, and the spatial extent of the inter-cluster magnetic interactions. These observations and conclusions have important implications for recent ideas on collective freezing of spin clusters in such alloys, and provide a starting point from which more extensive understanding of the phase behavior of the $Ni_{50-x}Co_xMn_{25+y}Sn_{25-y}$ system can be attained.

Acknowledgements: Work at UMN supported by IREE and DOE. DOE award DE-FG02-06ER46275 is specifically acknowledged for the neutron scattering component of the work. VS and RDJ acknowledge additional support from MURI (W911NF-07-1-0410) and NSF/PIRE (OISE-0967). Use of facilities at the UMN Institute for Rock Magnetism is also acknowledged. CL would like to thank F.S. Bates, J.A. Borchers and D. Phelan for useful discussions.

References

1. *Magnetism and Structure in Functional Materials*, Springer Series in Materials Science, vol. 79, Ed. A. Planes, L. Mañosa, and A. Saxena (Springer, New York, 2005).

2. T. Krenke, M. Acet, E.F. Wassermann, X. Moya, L. Manosa and A. Planes, Phys. Rev. B **72,** 014412 (2005).

3. T. Krenke, M. Acet, , E.F. Wassermann, X. Moya, L. Manosa and A. Planes, Phys. Rev B. **73,** 174413 (2006).

4. R.D. James and Z. Zhang, *A way to search for multiferroic materials with "unlikely" combinations of physical properties*, in *Magnetism and Structure in Functional Materials*, Springer Series in Materials Science, vol. 79, pp159, Ed. A. Planes, L. Mañosa, and A. Saxena (Springer, New York, 2005).

5. H.E. Karaca, I. Karaman, B. Basaran, Y Ren, Y.I. Chumlyakov and H.J. Maier, Adv. Funct. Mater. **19**, 983 (2009).

6. L. Manosa, D. Gonzalez-Alonso, A. Planes, E. Bonnot, M. Barrio, J.-L. Tamarit, S. Aksoy and M. Acet, Nat. Mat. **9** 478 (2010).

7. T. Krenke, E. Duman, M. Acet, E.F. Wassermann, X. Moya, L. Manosa and A. Planes, Nat. Mat. **4**, 450 (2005).

8. R. Kainuma, Y. Imano, W. Ito, Y. Sutou, H. Morito, S. Okamoto, O. Kitakami, K. Oikawa, A. Fujita, T. Kanomata and K. Ishida, Nature **439**, 957 (2006).

9. V. Srivastava, Y. Song, K.P. Bhatti and R. D. James, Adv. Energy Mater. **1,** 97 (2011).

10. Z. Zhang, R. D. James and S. Muller, Acta Mater. **57**, 4332 (2009); J. Cui, Y.S. Chu, O.O. Famodu, Y. Furuya, J. Hattrick-Simpers, R.D. James, A. Ludwig, S. Thienhaus, M. Wuttig, Z. Zhang and I. Takeuchi, Nat. Mat. **5**, 286 (2006); R. Zarnetta, R. Takahashi, M.L. Young, A.

Savan, Y. Furuya, S. Thienhaus, B. Maass, M. Rahim, J. Frenzel, H. Brunken, Y.S. Chu, V. Srivastava, R.D. James, I. Takeuchi, G. Eggeler and A. Ludwig, Adv. Func. Mater. **20,** 1917 (2010).

11. R. Delville, D. Schryvers, Z. Zhang, and R.D. James, Scripta Mater. **60**, 293 (2009).

12. V. Srivastava, X. Chen and R. D. James, Appl. Phys. Lett. **97**, 014101 (2010).

13. We note that NiMn is AF with a Néel temperature exceeding 1100 K.

14. M. Ye, A. Kimura, Y. Miura, M. Shirai, Y.T. Cui, K. Shimada, H. Namatame, M. Taniguchi, S. Ueda, K. Kobayashi, R. Kainuma, T. Shishido, K. Fukushima and T. Kanomata, Phys. Rev Lett. **104,** 176401 (2010).

15. P.J. Brown, A.P. Gandy, K. Ishida, R. Kainuma, T. Kanomata, K.-U. Neumann, K. Oikawa, B. Ouladdiaf and K.R.A. Ziebeck, J. Phys.: Condens. Matter **18**, 2249 (2006).

16. S. Aksoy, M.Acet, P. P. Deen, L. Manosa and A. Planes, Phys. Rev B **79**, 212401 (2009).

17. D.Y. Cong, S. Roth, M. Potschke, C. Hurrich and L. Schultz, Appl. Phys. Lett. **97**, 021908 (2010).

18. Although $Ni_{50}Mn_{39}Sn_{11}$ is labeled as paramagnetic in ref. 17, ref. 2 for instance, in agreement with other work and ref. 13, indicates an AF ground state at this composition.

19. D.Y. Cong, S. Roth, J. Liu, Q. Luo, M. Potschke, C. Hurrich and L. Schultz, Appl. Phys. Lett. **96**, 112504 (2010).

20. B.M. Wang, Y. Liu, P. Ren, B. Xia, K.B. Ruan, J.B. Yi, J. Ding, X.G. Li and L. Wang, Phys. Rev. Lett. **106,** 077203 (2011).

21. M. Khan, I. Dubenko, S. Stadler and N. Ali, Appl. Phys. Lett. **91**, 072510 (2007).

22. Z. Li, C. Jing, J. Chen, S. Yuan, S. Cao and J. Zhang, Appl. Phys. Lett. **91**, 112505 (2007).

23. Y. Song, K.P. Bhatti, V. Srivastava, C. Leighton and R. D. James, in preparation (2012).

24. T. Krenke, E. Duman, M. Acet, X. Moya, L. Manosa and A. Planes, J. Appl. Phys. **102**, 033903 (2007).

25. S.Y. Yu, Z.X. Cao, L. Ma, G.D. Liu, J.L. Chen, G.H. Wu, B. Zhang and X.X. Zhang, Appl. Phys. Lett. **91**, 102507 (2007).

26. W. Ito, X. Xu, R.Y. Umestu, T. Kanomata, K. Ishida and R. Kainuma, Appl. Phys. Lett. **97**, 242512 (2010).

27. R.Y. Umetsu, A. Sheikh, W. Ito, B. Ouladdiaf, K.R.A. Ziebeck, T. Kanomata, and R. Kainuma, Appl. Phys. Lett. 98, 042507 (2011).

28. R.C. O'Handley, *Modern Magnetic Materials: Principles and Applications*, Wiley, New York (2000).

29. J. Nogues and I.K. Schuller, J. Mag. Mag. Mat. **192**, 203 (1999).

30. J.W. Cai, K. Liu and C.L. Chien, Phys. Rev. B. **60**, 72 (1999).

31. C. Leighton, M.R. Fitzsimmons, A. Hoffmann, J. Dura, C.F. Majkrzak, M.S. Lund and I.K. Schuller, Phys. Rev. B. **65**, 064403 (2002).

32. This must be distinguished from the case of AF interfacial interactions which leads to more complex dependence on the cooling field (see ref. 29 for more details).

33. B.T.M. Willis and C.J. Carlile, *Experimental Neutron Scattering*, Oxford University Press, Oxford (2009).

34. See for instance, A. Kreyssig, R. Prozorov, C.D. Dewhurst, P.C. Canfield, R.W. McCallum and A.I. Goldman, Phys. Rev. Lett. **102**, 047204 (2009).

35. A. Furrer, J. Mesot and T. Strassle, *Neutron Scattering in Condensed Matter Physics*, World Scientific, Singapore (2009).

36. S.W. Lovesey, *Theory of Neutron Scattering from Condensed Matter*, Clarendon Press, Oxford (1984).

37. W. Wagner and J. Kohlbrecker, *Small-Angle Neutron Scattering (SANS)*, in *Modern Techniques for Characterizing Magnetic Materials*, pp. 65, Springer, New York (2005).

38. D.F. Farrell, Y. Ijiri, C.V. Kelly, J.A. Borchers, J.J. Rhyne, Y. Ding and S.A. Majetich, J. Mag. Mag. Mat. **303**, 318 (2006)

39. M. Sachan, C. Bonnoit, S.A. Majetich, Y. Ijiri, P.O. Mensah-Bonsu, J.A. Borchers and J.J. Rhyne, Appl. Phys. Lett. **92**, 152503 (2008).

40. E. Granado, C.D. Ling, J.J. Neumeier, J.W. Lynn and D.N. Argyriou, Phys. Rev. B. **68**, 134440 (2003).

41. M. Hennion, F. Moussa, G. Biotteau, J. Rodriguez-Carvajal, L. Pinsard and A. Revcolevschi, Phys. Rev. Lett. **81**, 1957 (1998).

42. N.W. Ashcroft and J. Lekner, Phys. Rev. **145**, 83 (1966).

43. S. Sankar, D. Dender, J.A. Borchers, D.J. Smith, R.W. Erwin, S.R. Kline and A.E. Berkowitz, J. Mag. Mag. Mat. **221,** 1 (2000)

44. E. Dagotto, *Nanoscale phase separation and colossal magnetoresistance*, Springer, New York (2002).

45. E. Dagotto, T. Hotta and A. Moreo, Phys. Rep. **344**, 1 (2001).

46. See the following reference as an example where subtle compositional fluctuations drive the nanoscopic magnetic phase separation: C. He, S. El-Khatib, J. Wu, J.W. Lynn, H. Zheng, J.F. Mitchell and C. Leighton, Europhys. Lett. **87,** 27006 (2009).

Figure captions

Figure 1 (color online): Wide-angle x-ray diffraction patterns from $Ni_{44}Co_6Mn_{40}Sn_{10}$ at (a) T = 410 K and (b) T = 300 K, i.e. above and below the martensitic phase transformation respectively. Heavy and light solid lines represent experimental data and the structural refinement, respectively. The dotted line shows the residual between the experiment and model.

Figure 2 (color online): Temperature dependence (5 - 600 K) of the zero field cool warming (ZFCW) and field cool cooling (FCC) magnetization of $Ni_{44}Co_6Mn_{40}Sn_{10}$ at applied magnetic fields of (a) 10 Oe, (b) 5 kOe, (c) 40 kOe, and (d) 70 kOe. The inset to (a) shows an enlarged view of the low temperature (5 – 300 K) region of the 10 Oe data.

Figure 3 (color online): Isothermal magnetization hysteresis loops of $Ni_{44}Co_6Mn_{40}Sn_{10}$ at (a) 550 and 415 K (above the martensitic phase transformation), (b) 400, 395 and 390 K (the transition region), (c) 370, 300, 200, 150, 100 and 80 K (below the martensitic phase transformation), and (d) 30 and 5 K (the superparamagnetic blocking region). The inset to (a) shows an enlarged view of the 415 K data, demonstrating hysteresis and remnance. In (c) the solid lines are fits to the model described in the text (equation (1)). The data were taken after warming to 600 K then cooling to the measurement temperature.

Figure 4 (color online): Temperature dependence (60 – 370 K) of the parameters extracted from fitting of the field dependence of the magnetization of $Ni_{44}Co_6Mn_{40}Sn_{10}$ (Fig. 3(c)). These parameters are (a) the susceptibility of the non-ferromagnetic matrix, (b) the magnetization of

individual clusters, and (c) the cluster density. The vertical dashed line around 125 K marks the transition between two regimes as discussed in the text.

Figure 5 (color online): (a) Magnetization hysteresis loops at 5 K measured after field cooling from 300 K in +10 kOe and -10 kOe. (b) Temperature dependence of the coercivity (left axis) and exchange bias (right axis) after field cooling from 300 K in 70 kOe. (c) Cooling field dependence of the 5 K coercivity and exchange bias. All data are for $Ni_{44}Co_6Mn_{40}Sn_{10}$.

Figure 6 (color online): Scattering wavevector dependence of the absolute SANS cross section from $Ni_{44}Co_6Mn_{40}Sn_{10}$ at (a) 500 K, (b) 425 K, (c) 390 K, (d) 380 K, and (e) 30 K. The points are experimental data (with error bars). The heavy solid line is the overall fit, while the lighter solid, dotted and dashed lines represent the individual Porod, Gaussian, and Lorentzian contributions, as defined in equations (2) to (4). The data were taken sequentially, on warming.

Figure 7 (color online): Temperature dependence (30 – 500 K) of the SANS cross section from $Ni_{44}Co_6Mn_{40}Sn_{10}$ at a scattering wavevector of (a) 0.005 $Å^{-1}$ and (b) 0.1 $Å^{-1}$. Data taken on both heating (black solid points) and cooling (red open points) are shown (with error bars). The inset to (b) shows an enlarged view of the 0.1 $Å^{-1}$ data at low *T* (i.e. below 300 K). The dashed line is a guide to the eye.

Figure 8 (color online): Temperature dependence (cooling and warming) of the parameters extracted from the SANS data presented in Fig. 6; (a) the Porod contribution, (b) the Porod exponent, (c) the Lorentzian contribution, (d) the magnetic correlation length, (e) the Gaussian

contribution, and (f) the position (left axis) and width (right axis) of the Gaussian peak. In (d) the solid line is a fit to the equation described in the text. In (e) the inset is an enlarged view of the low temperature region.

Figure 9 (color online): Temperature dependence for $Ni_{42}Co_8Mn_{40}Sn_{10}$ of the zero field cool warming (ZFCW) and field cool cooling (FCC) magnetization at an applied magnetic field of 5 kOe (a), the SANS cross section at scattering wavevector of 0.01 $Å^{-1}$ (b) and 0.1 Å (c), and the magnetic correlation length (d). The data for parts (b)-(d) were taken on cooling only. In (d) the solid line is a fit to the equation described in the text.

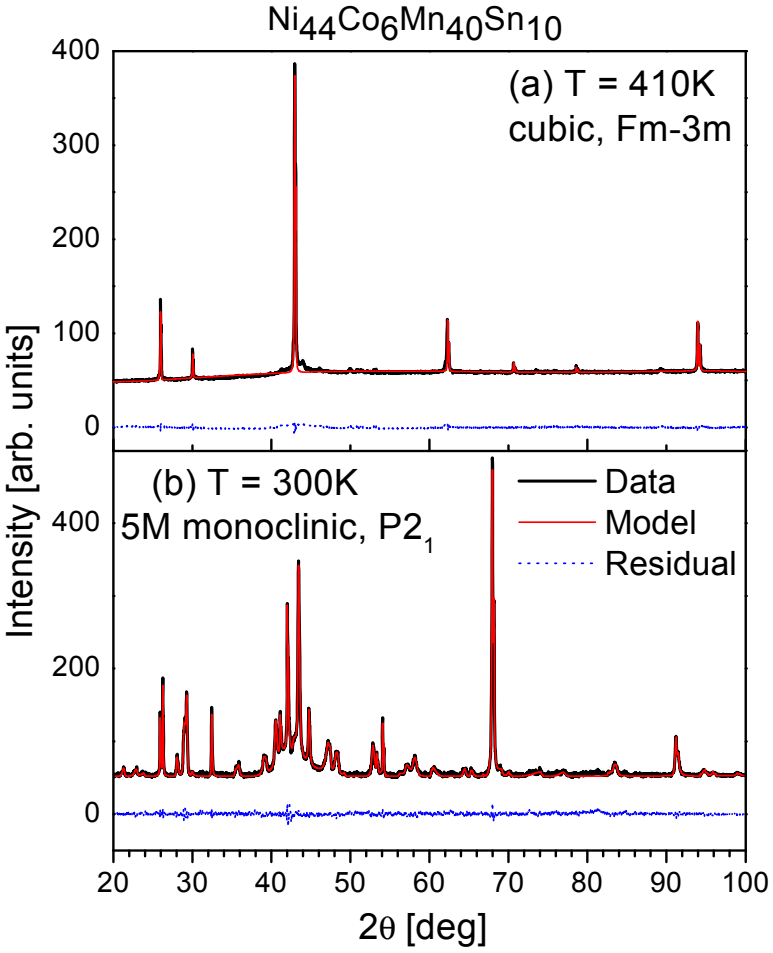
Ni44Co6Mn40Sn10
(a) T = 410K
cubic, Fm-3m
(b) T = 300K
5M monoclinic, P21
Data
Model
Residual
Intensity [arb. units]
2θ [deg]
0
100
200
300
400
20
30
40
50
60
70
80
90
100

Figure 1

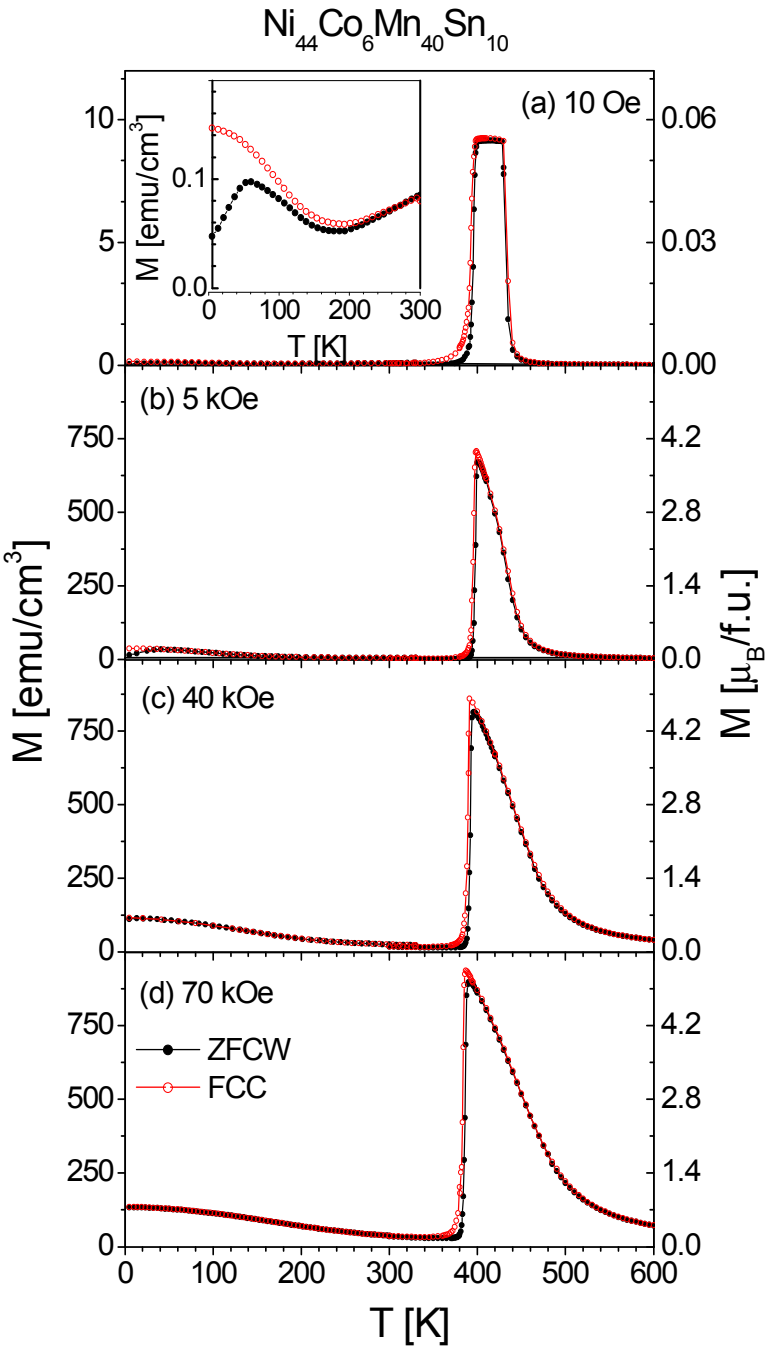
Ni44Co6Mn40Sn10
(a) 10 Oe
M [emu/cm3]
T [K]
(b) 5 kOe
(c) 40 kOe
(d) 70 kOe
ZFCW
FCC
M [emu/cm3]
M [μB/f.u.]
T [K]

Figure 2

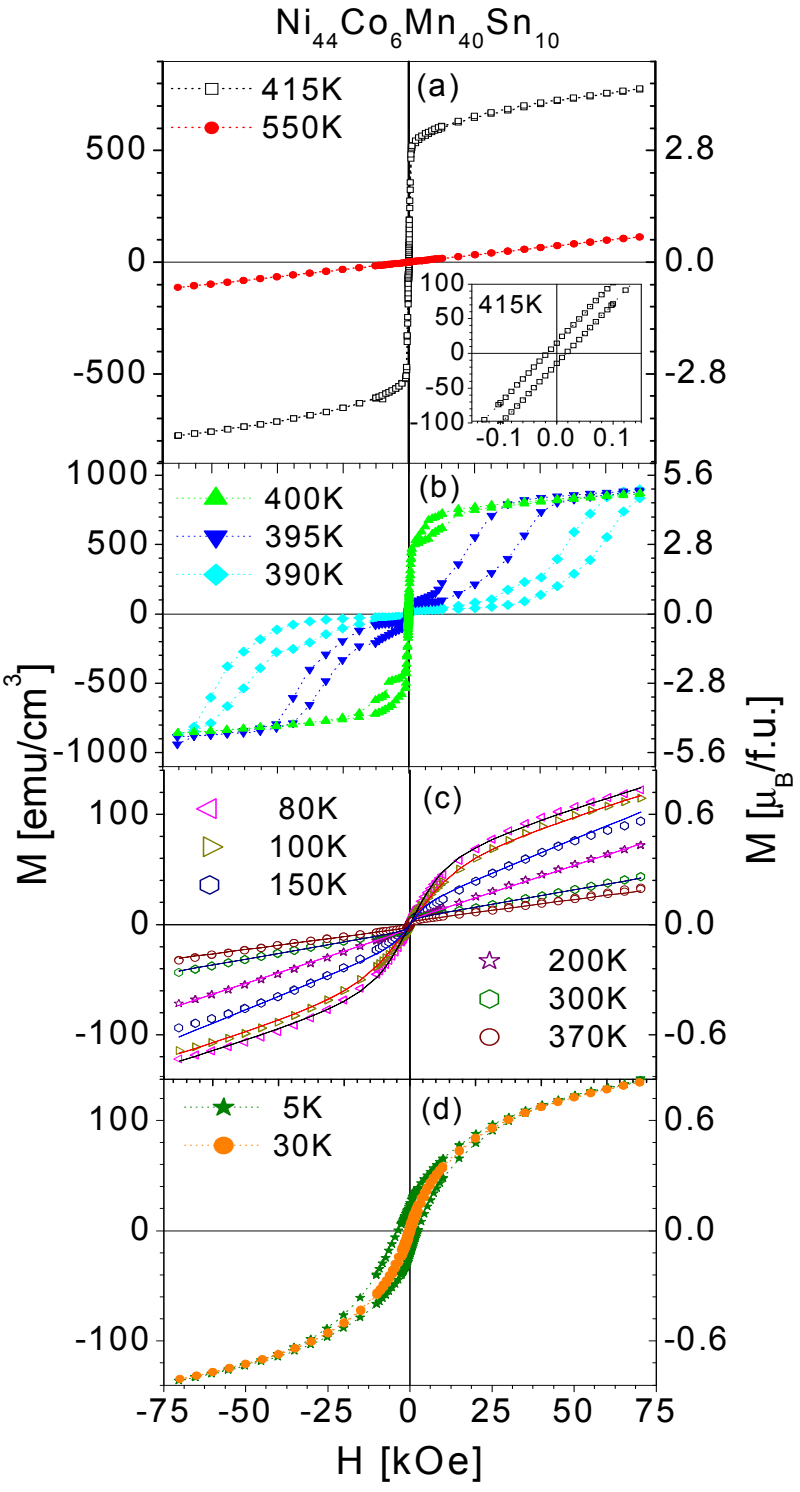
Ni44Co6Mn40Sn10
415K
550K
(a)
415K
400K
395K
390K
(b)
80K
100K
150K
(c)
200K
300K
370K
5K
30K
(d)
M [emu/cm3]
M [μB/f.u.]
H [kOe]

Figure 3

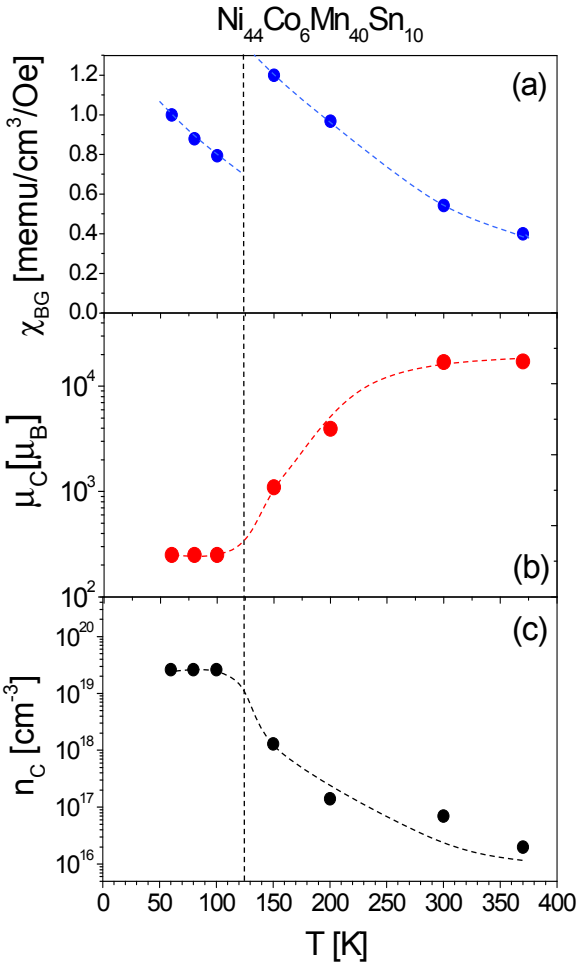

Figure 4

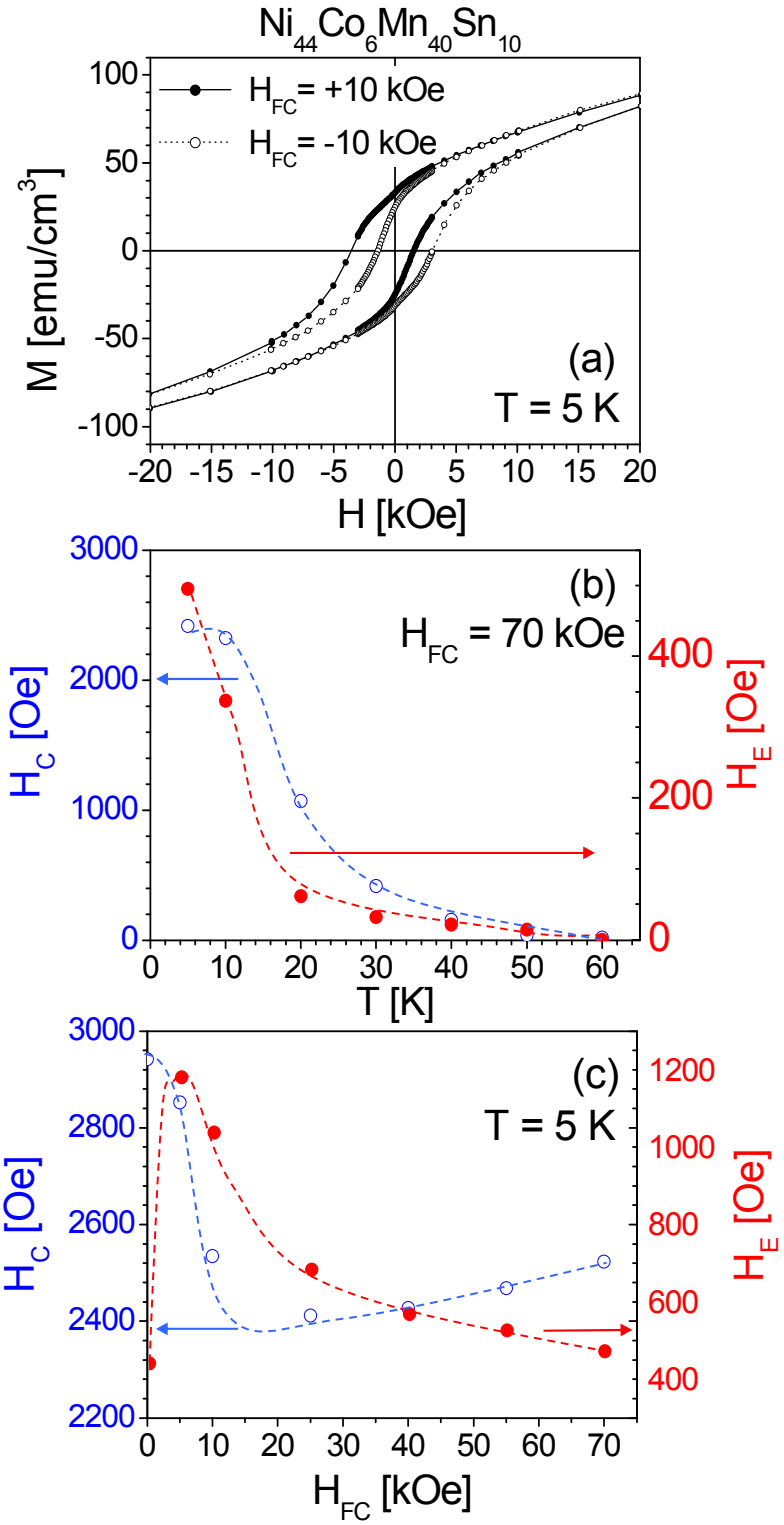
Ni44Co6Mn40Sn10
HFC= +10 kOe
HFC= -10 kOe
M [emu/cm3]
H [kOe]
(a)
T = 5 K
(b)
HFC = 70 kOe
HC [Oe]
HE [Oe]
T [K]
(c)
T = 5 K
HFC [kOe]

Figure 5

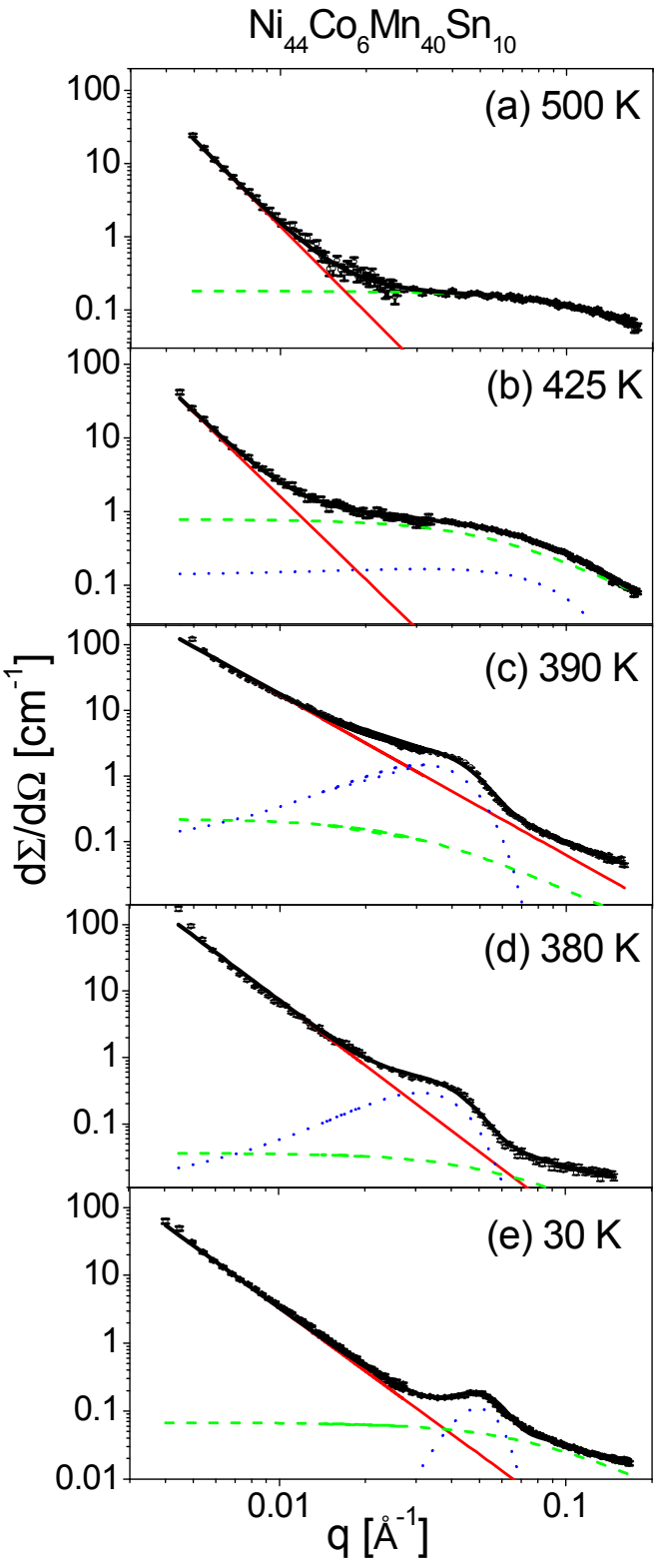
Ni44Co6Mn40Sn10
(a) 500 K
(b) 425 K
(c) 390 K
(d) 380 K
(e) 30 K
dΣ/dΩ [cm-1]
q [Å-1]
100
10
1
0.1
0.01
0.01
0.1

Figure 6

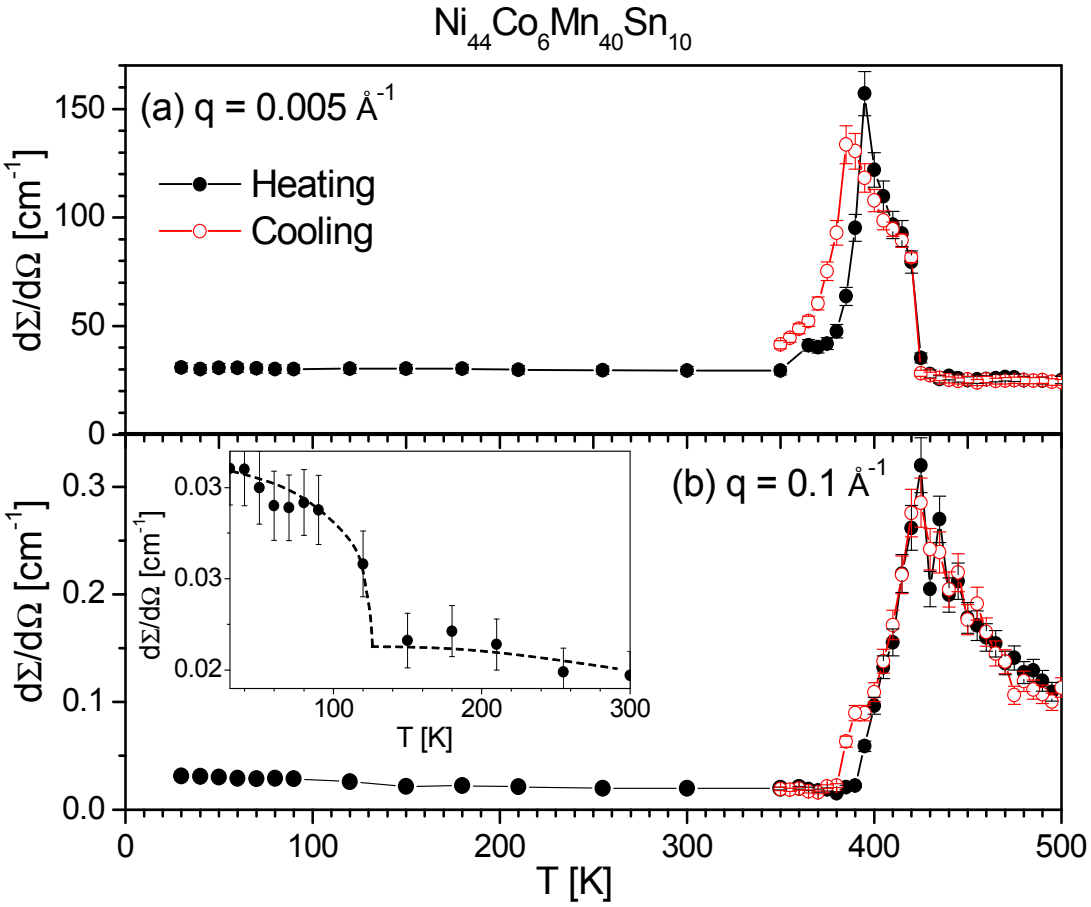
Ni44Co6Mn40Sn10
(a) q = 0.005 Å-1
Heating
Cooling
dΣ/dΩ [cm-1]
150
100
50
0
(b) q = 0.1 Å-1
dΣ/dΩ [cm-1]
0.3
0.2
0.1
0.0
0.03
0.03
0.02
100
200
300
T [K]
0
100
200
300
400
500
T [K]

Figure 7

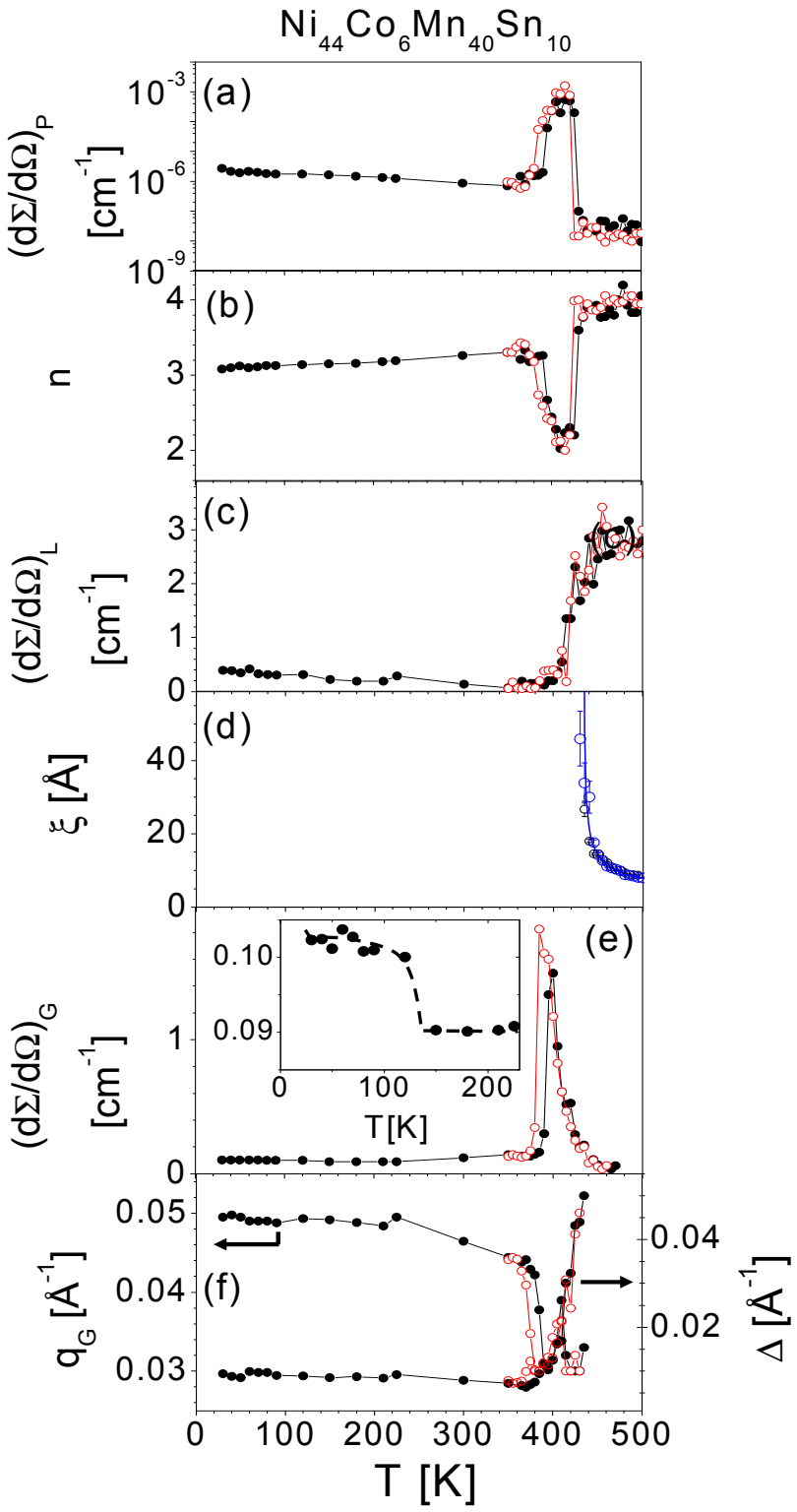
Ni44Co6Mn40Sn10
(a)
(b)
(c)
(d)
(e)
(f)
(dΣ/dΩ)P [cm-1]
n
(dΣ/dΩ)L [cm-1]
ξ [Å]
(dΣ/dΩ)G [cm-1]
T[K]
qG [Å-1]
Δ [Å-1]
T [K]

Figure 8

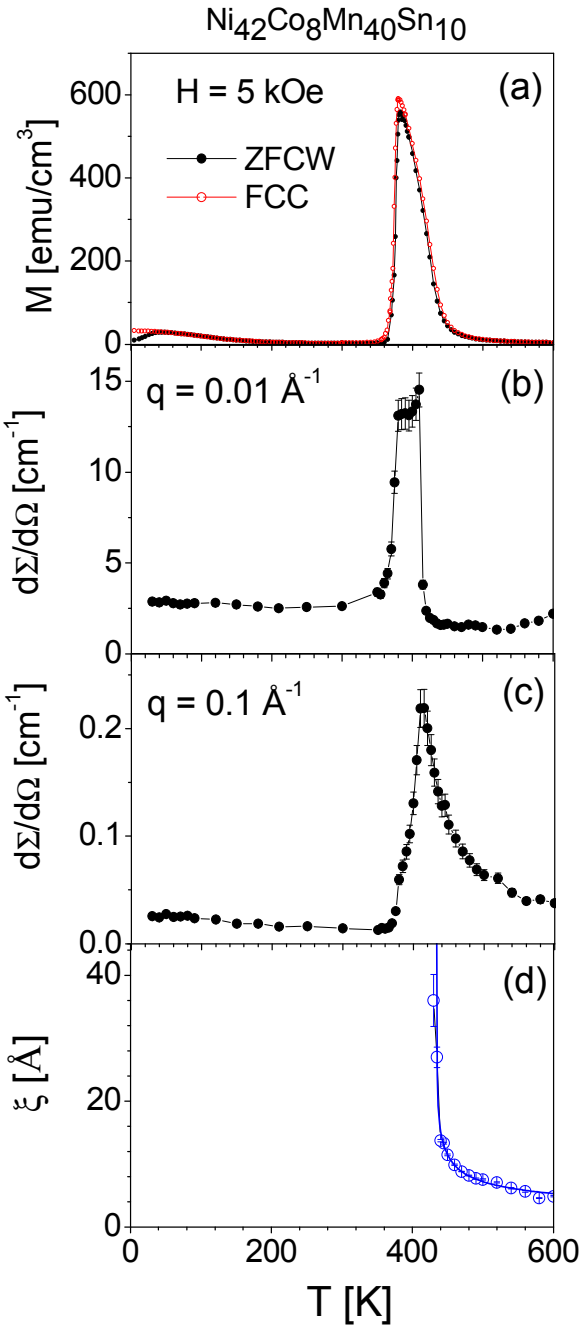
Ni42Co8Mn40Sn10
H = 5 kOe
(a)
ZFCW
FCC
M [emu/cm3]
600
400
200
0
q = 0.01 Å-1
(b)
dΣ/dΩ [cm-1]
15
10
5
0
q = 0.1 Å-1
(c)
dΣ/dΩ [cm-1]
0.2
0.1
0.0
(d)
ξ [Å]
40
20
0
0
200
400
600
T [K]

Figure 9